

Alexander L. Kalamkarov

alex.kalamkarov@dal.ca
Dalhousie University
Department of Mechanical Engineering
B3H 4R2 Halifax, Nova Scotia, Canada

Marcelo A. Savi

savi@mecanica.ufrrj.br
Universidade Federal do Rio de Janeiro
COPPE – Department of Mechanical Engineering
68503 Rio de Janeiro, RJ, Brazil

Micromechanical Modeling and Effective Properties of the Smart Grid-Reinforced Composites

Smart composite structures reinforced with a periodic grid of generally orthotropic cylindrical reinforcements that also exhibit piezoelectric behavior are analyzed using the asymptotic homogenization method. The analytical expressions for the effective elastic and piezoelectric coefficients are derived. In particular, the smart orthotropic composite structures with cubic, conical and diagonal actuator and reinforcement orientations are investigated.

Keywords: smart grid-reinforced composite, asymptotic homogenization, effective properties

Introduction

The mechanical modeling of composite structures made of reinforcements embedded in a matrix has been the focus of investigation for some time. Noteworthy among the earlier models is the composite cylinders model proposed by Hashin and Rosen (1964). Budiansky (1965) developed a model which predicted the elastic moduli of multiphase composites with isotropic constituents. Other work can be found in Mori and Tanaka (1973), Sendekyj (1974), Vinson and Sierokowski (1986), Christensen (1990), Drugan and Willis (1996), Kalamkarov and Liu (1998), Andrianov et al. (2006) and others.

Micromechanical models for the smart composites must take into consideration both local and global properties. Accordingly, the developed models should be rigorous enough to enable the consideration of the spatial distribution, mechanical properties, and behavior of the different constituents (reinforcing elements, matrix and actuators) at the local level, but not too complex to be described and used via straightforward analytical and numerical approaches.

Effective technique that can be used for the analysis of smart composites with regular structures is the multi-scale asymptotic homogenization method. The mathematical framework of this method can be found in Bensoussan et al. (1978), Sanchez-Palencia (1980), Bakhvalov and Panasenko (1984), Kalamkarov (1992). This method is mathematically rigorous and it enables the prediction of both the local and global effective properties of the periodic composite structure. Many problems in the framework of elasticity and thermoelasticity have been solved using this approach. For example, Kalamkarov and Georgiades developed general micromechanical models pertaining to smart composite structures with homogeneous (2002a) and non-homogeneous (2002b) structural boundary conditions, the later resulting in a boundary-layer type solution. Kalamkarov (1992) developed comprehensive micromechanical model for a thin composite layer with wavy upper and lower surfaces. This model was subsequently used to analyze the wafer and rib-reinforced smart composite plates as well as the sandwich composites with honeycomb fillers, see, e.g., Kalamkarov and Kolpakov (1997, 2001), Kalamkarov et al. (2009a). More recently, Kalamkarov et al. (2006), Georgiades et al. (2006) and Challagulla et al. (2007, 2008) have determined effective coefficients for the network-reinforced composite plates and shells. Saha et al. (2007a,b) investigated the smart composite sandwich shells made of generally orthotropic materials. The objective of these studies was to transform a general anisotropic composite material with a periodic array of reinforcements and actuators into a simpler one that is characterized by some effective coefficients. It is implicit of course that the physical problem based on these effective

coefficients should give predictions differing as little as possible from those of the original problem.

The micromechanical models for the composite structures reinforced with a periodic grid of generally orthotropic cylindrical reinforcements have been developed in Kalamkarov et al. (2009b, 2010), Hassan et al. (2011), Hassan et al. (2009) and Hassan (2011) investigated smart grid-reinforced composite structures.

The review of micromechanical modeling of smart grid-reinforced structures based on the application of the asymptotic homogenization method is presented in the present paper. The formulated model is subsequently used to evaluate the effective elastic and piezoelectric coefficients of such structures.

Following this introduction the rest of the paper is organized as follows. The basic problem formulation is presented in the next section. That is then followed by the general piezoelectric model pertaining to smart 3D grid-reinforced composite structures with generally orthotropic reinforcements and actuators. The micromechanical model is further illustrated by means of several practically-important examples.

Nomenclature

σ_{ij}	= stress tensor
e_{kl}	= strain tensor
u_i	= displacement field
C_{ijkl}	= tensor of elastic coefficients
P_{ijk}	= tensor of piezoelectric coefficients
R	= control signal
f_i	= body forces
ε	= small parameter characterizing dimension of a unit cell Y , dimensionless
\tilde{C}_{ijkl}	= effective elastic coefficients
\tilde{P}_{ijk}	= effective piezoelectric coefficients

Asymptotic Homogenization Model for 3D Composite Structures

Consider a smart composite structure in a form of an inhomogeneous solid occupying domain Ω with boundary $\partial\Omega$ that contains a large number of periodically arranged reinforcements and actuators, see Fig. 1(a). It can be observed that this periodic structure is obtained by repeating a small unit cell Y in the domain Ω , see Fig. 1(b).

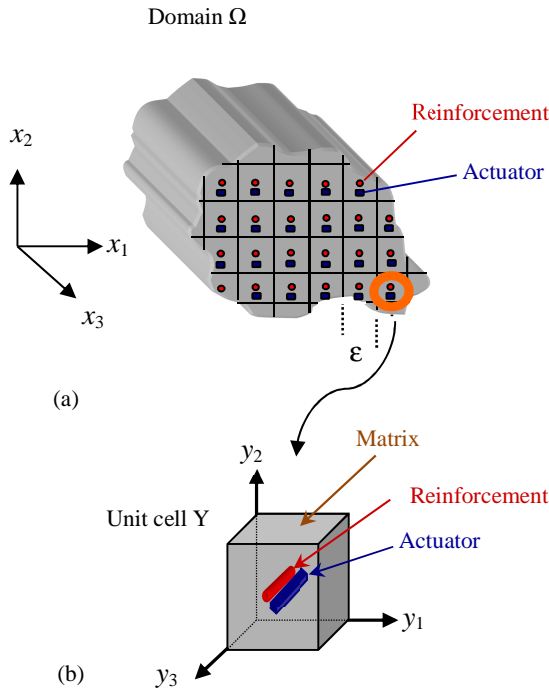


Figure 1. (a) 3D smart composite solid of a regular structure and (b) unit cell Y .

The elastic deformation of this structure can be described by the following boundary-value problem:

$$\frac{\partial \sigma_{ij}}{\partial x_j} = f_i \text{ in } \Omega, \quad u_i(\mathbf{x}) = 0 \text{ on } \partial\Omega, \quad (1)$$

$$\sigma_{ij} = C_{ijkl} e_{kl} - P_{ijk} R_k(\mathbf{x}), \quad e_{ij} = \frac{1}{2} \left(\frac{\partial u_i}{\partial x_j} + \frac{\partial u_j}{\partial x_i} \right) \quad (2)$$

In Eqs. (1) and (2) and in the sequel all indices assume values 1,2,3 and the summation convention is adopted, C_{ijkl} is the tensor of elastic coefficients, e_{kl} is the strain tensor which is a function of the displacement field u_i , P_{ijk} is a tensor of piezoelectric coefficients describing the effect of a control signal R on the stress field σ_{ij} . Finally, f_i represent body forces. Note that the present analysis is limited by considering only converse piezoelectric effect. This limitation does not affect the derived formulae for the effective elastic and piezoelectric coefficients of the smart grid-reinforced composite structure.

It is assumed in Eq. (1) that all the elastic and piezoelectric coefficients are periodic functions of spatial coordinates with a unit cell Y of characteristic dimension ε . Small parameter ε is made non-dimensional by dividing the size of the unit cell by a certain characteristic dimension of the overall structure.

The development of asymptotic homogenization model for the 3D smart composite structures can be found in Kalamkarov (1992), Kalamkarov et al. (2009a,b), Hassan et al. (2009). Here a brief review of the steps involved in the development of the model is given.

The first step is to define the so-called ‘‘fast’’ or microscopic variables according to:

$$y_1 = x_1/\varepsilon, \quad y_2 = x_2/\varepsilon, \quad y_3 = x_3/\varepsilon \quad (3)$$

As a consequence of introducing y coordinates, the derivatives are also transformed according to

$$\begin{aligned} \frac{\partial}{\partial x_1} &\rightarrow \frac{\partial}{\partial x_1} + \frac{1}{\varepsilon} \frac{\partial}{\partial y_1}, & \frac{\partial}{\partial x_2} &\rightarrow \frac{\partial}{\partial x_2} + \frac{1}{\varepsilon} \frac{\partial}{\partial y_2}, \\ \frac{\partial}{\partial x_3} &\rightarrow \frac{\partial}{\partial x_3} + \frac{1}{\varepsilon} \frac{\partial}{\partial y_3} \end{aligned} \quad (4)$$

The boundary value problem and corresponding stress field defined in Eqs. (1) and (2) are thus transformed into the following expressions:

$$\frac{\partial \sigma_{ij}(\mathbf{x}, \mathbf{y})}{\partial x_j} + \frac{1}{\varepsilon} \frac{\partial \sigma_{ij}(\mathbf{x}, \mathbf{y})}{\partial y_i} = f_i \text{ in } \Omega, \quad (5)$$

$$u_i(\mathbf{x}, \mathbf{y}) = 0 \text{ on } \partial\Omega$$

$$\sigma_{ij}(\mathbf{x}, \mathbf{y}) = C_{ijkl}(\mathbf{y}) \frac{\partial u_k}{\partial x_l}(\mathbf{x}, \mathbf{y}) - P_{ijk}(\mathbf{y}) R_k(\mathbf{x}) \quad (6)$$

The next step is to consider the following asymptotic expansions in terms of powers of the small parameter ε :

$$u_i(\mathbf{x}, \mathbf{y}) = u_i^{(0)}(\mathbf{x}, \mathbf{y}) + \varepsilon u_i^{(1)}(\mathbf{x}, \mathbf{y}) + \varepsilon^2 u_i^{(2)}(\mathbf{x}, \mathbf{y}) + \dots \quad (7)$$

$$\sigma_i(\mathbf{x}, \mathbf{y}) = \sigma_i^{(0)}(\mathbf{x}, \mathbf{y}) + \varepsilon \sigma_i^{(1)}(\mathbf{x}, \mathbf{y}) + \varepsilon^2 \sigma_i^{(2)}(\mathbf{x}, \mathbf{y}) + \dots \quad (8)$$

By substituting Eqs. (7) and (8) into Eqs. (5) and (6) and considering at the same time the periodicity of $u^{(i)}$ in y one can readily eliminate the microscopic variable y from the first term $u^{(0)}$ in the asymptotic displacement field expansion thus showing that it depends only on the macroscopic variable x . Subsequently, by separating terms with like powers of ε one obtains a series of differential equations, the first two of which are:

$$\frac{\partial \sigma_{ij}^{(0)}}{\partial y_j} = 0 \quad (9a)$$

$$\frac{\partial \sigma_{ij}^{(1)}}{\partial y_j} + \frac{\partial \sigma_{ij}^{(0)}}{\partial x_j} = f_i \quad (9b)$$

where

$$\sigma_{ij}^{(0)} = C_{ijkl} \left(\frac{\partial u_k^{(0)}}{\partial x_l} + \frac{\partial u_k^{(1)}}{\partial y_l} \right) - P_{ijk} R_k \quad (10a)$$

$$\sigma_{ij}^{(1)} = C_{ijkl} \left(\frac{\partial u_k^{(1)}}{\partial x_l} + \frac{\partial u_k^{(2)}}{\partial y_l} \right) \quad (10b)$$

Combination of Eqs. (9a) and (10a) leads to the following expression:

$$\frac{\partial}{\partial y_j} \left(C_{ijkl} \frac{\partial u_k^{(1)}(\mathbf{x}, \mathbf{y})}{\partial y_l} \right) = \frac{\partial P_{ijk}(\mathbf{y})}{\partial y_j} R_k(\mathbf{x}) - \frac{\partial C_{ijkl}(\mathbf{y})}{\partial y_j} \frac{\partial u_k^{(0)}(\mathbf{x})}{\partial x_l} \quad (11)$$

The separation of variables in the right-hand-side of Eq. (11) prompts to represent the solution for $u^{(1)}$ as:

$$u_m^{(1)}(\mathbf{x}, \mathbf{y}) = \frac{\partial u_k^{(1)}(\mathbf{x})}{\partial x_l} N_m^{kl}(\mathbf{y}) + R_k(\mathbf{x}) M_m^k(\mathbf{y}) \quad (12)$$

where the auxiliary functions N_m^{kl} and M_m^k are periodic in \mathbf{y} and they satisfy the following problems:

$$\frac{\partial}{\partial y_j} \left(C_{ijmn}(\mathbf{y}) \frac{\partial N_m^{kl}(\mathbf{y})}{\partial y_n} \right) = -\frac{\partial C_{ijkl}}{\partial y_j} \quad (13)$$

$$\frac{\partial}{\partial y_j} \left(C_{ijmn}(\mathbf{y}) \frac{\partial M_m^k(\mathbf{y})}{\partial y_n} \right) = \frac{\partial P_{ijk}}{\partial y_j} \quad (14)$$

One observes that Eqs. (13) and (14) depend only on the fast variable \mathbf{y} and thus are formulated in the domain Y of the unit cell, remembering at the same time that all of C_{ijkl} , P_{ijk} and N_m^{kl} and M_m^k are Y -periodic in \mathbf{y} . Consequently, Eqs. (13) and (14) are appropriately called the unit-cell problems.

The next important step in the model development is the homogenization procedure. This is carried out by first substituting Eq. (12) into Eq. (10a), and combining the result with Eq. (9b). The resulting expressions are then integrated over the unit cell Y (with the volume $|Y|$) remembering to treat \mathbf{x} as a parameter as far as integration with respect to \mathbf{y} is concerned. After cancelling the terms that vanish due to periodicity, this yields the following equation:

$$\tilde{C}_{ijkl} \frac{\partial^2 u_k^{(0)}(\mathbf{x})}{\partial x_j \partial x_l} - \tilde{P}_{ijk} \frac{\partial R_k(\mathbf{x})}{\partial x_j} = f_i \quad (15)$$

where the following definitions are introduced:

$$\tilde{C}_{ijkl} = \frac{1}{|Y|} \int_Y \left(C_{ijkl}(\mathbf{y}) + C_{ijmn}(\mathbf{y}) \frac{\partial N_m^{kl}(\mathbf{y})}{\partial y_n} \right) d\mathbf{v} \quad (16)$$

$$\tilde{P}_{ijk} = \frac{1}{|Y|} \int_Y \left(P_{ijk}(\mathbf{y}) - C_{ijmn}(\mathbf{y}) \frac{\partial M_m^k(\mathbf{y})}{\partial y_n} \right) d\mathbf{v} \quad (17)$$

Coefficients \tilde{C}_{ijkl} , \tilde{P}_{ijk} defined by Eqs. (16) and (17) are the effective elastic and piezoelectric coefficients respectively. It is noticed that they are constant unlike their original rapidly varying

material counterparts C_{ijkl} , P_{ijk} and therefore problem (15) is much simpler than the original problem given by Eqs. (5) and (6). It is worth mentioning that although the present work pertains to piezoelectric actuators, the model derived applies equally well if the smart composite structure is associated with some general transduction properties that can be used to induce residual strains and stresses. In that case, the coefficients \tilde{P}_{ijk} represent the appropriate effective actuation coefficients (rather than the piezoelectric ones).

3D Smart Grid-Reinforced Composite Structures

In the subsequent Sections we will consider the problem of a smart 3D composite structure reinforced with N families of reinforcements/actuators, see for example Fig. 2 where an explicit case of multiple families of reinforcements is shown.

We assume that the members of each family are made of different generally orthotropic materials that may exhibit piezoelectric characteristics and that the reinforcements of each family make angles $\phi_1^n, \phi_2^n, \phi_3^n$ ($n = 1, 2, \dots, N$) with the y_1, y_2, y_3 axes respectively. It is further assumed that the orthotropic reinforcements/actuators have significantly larger elastic moduli than the matrix material, so we are justified in neglecting the contribution of the matrix phase in the ensuing analytical treatment. The error resulting from this simplifying assumption is discussed below. Clearly, for the case of the lattice grid structures there is no surrounding matrix and assumption of zero matrix rigidity is exact.

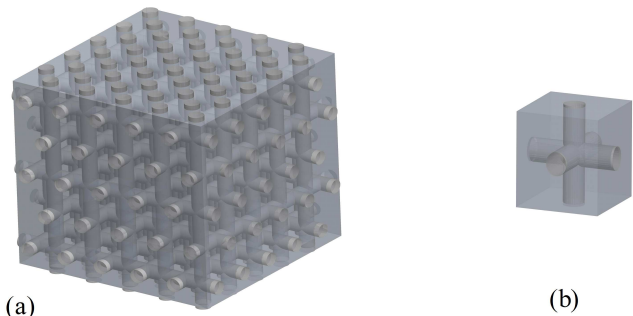


Figure 2. (a) 3D grid-reinforced smart composite structure and (b) its unit cell.

The nature of the grid-reinforced composite structure of Fig. 2 is such that it would be more efficient if we first considered a simpler type of unit cell made of only a single reinforcement/actuator as shown in Fig. 3. Having dealt with this situation, the effective elastic and piezoelectric coefficients of more general structures with multiple families of reinforcements/actuators can be determined by superposition of the solution for each of them found separately. In following this procedure, one must naturally accept the error incurred at the regions of intersection between the reinforcements. However, our approximation will be quite accurate since these regions of intersection are highly localized and do not contribute significantly to the integral over the entire volume of the unit cell. Essentially, the error incurred will be negligible if the dimensions of the actuators/reinforcements are much smaller than the spacing between them. The mathematical justification for this argument in the form of the so-called principle of the split homogenized operator can be found in Bakhvalov and Panasenko (1989).

In order to evaluate the accuracy of the above two key assumptions pertaining to the asymptotic model, the finite element analysis was carried out in Hassan et al. (2011). It is shown that

errors in the values of the effective properties are negligibly small for a large mismatch between the stiffness of the reinforcements and the matrix. The finite element results have also indicated that the error from ignoring the regions of overlap of reinforcements will only be significant for the cases of grid-reinforced structures with more than three different reinforcement families; if the unit cell consists of up to three different reinforcements the associated error is negligibly small.

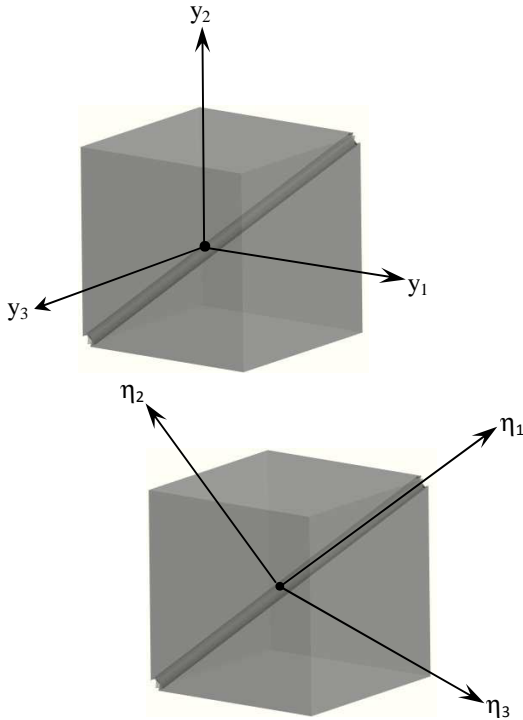


Figure 3. Unit cell in case of a single reinforcement family in the original and rotated microscopic coordinates.

In order to calculate the effective coefficients for the simpler structure of Fig. 3, unit cell problems given by Eqs. (13) and (14) should be solved and, subsequently, Eqs. (16) and (17) should be applied.

The problem formulation for the structure shown in Fig. 3 begins with the introduction of the following local functions:

$$b_{ij}^{kl} = C_{ijkl}(\mathbf{y}) + C_{ijmn}(\mathbf{y}) \frac{\partial N_m^{kl}(\mathbf{y})}{\partial y_n} \quad (18)$$

$$p_{ij}^k = P_{ijk}(\mathbf{y}) - C_{ijmn}(\mathbf{y}) \frac{\partial M_m^k(\mathbf{y})}{\partial y_n} \quad (19)$$

The unit cell problems in Eqs. (13) and (14) can be then written as follows:

$$\frac{\partial}{\partial y_j} b_{ij}^{kl} = 0 \quad (20)$$

$$\frac{\partial}{\partial y_j} p_{ij}^k = 0 \quad (21)$$

Perfect bonding conditions are assumed at the interfaces between the actuators/reinforcements and the matrix. This assumption yields the following interface conditions:

$$N_n^{kl}(\mathbf{r})|_s = N_n^{kl}(\mathbf{m})|_s, \quad b_{ij}^{kl}(\mathbf{r})n_j|_s = b_{ij}^{kl}(\mathbf{m})n_j|_s \quad (22)$$

$$M_n^k(\mathbf{r})|_s = M_n^k(\mathbf{m})|_s, \quad p_{ij}^k(\mathbf{r})n_j|_s = p_{ij}^k(\mathbf{m})n_j|_s \quad (23)$$

In Eqs. (22) and (23) “ r ”, “ m ”, and “ s ” denote the actuator/reinforcement, matrix, and reinforcement/matrix interface, respectively; while n_j denote the components of the unit normal vector at the interface. As was mentioned earlier, we will further assume that $C_{ijkl}(\mathbf{m}) = 0$, which implies from Eqs. (18) and (19)

that $b_{ij}^{kl}(\mathbf{m}) = p_{ij}^k(\mathbf{m}) = 0$. Therefore, the interface conditions in Eqs. (22) and (23) become

$$b_{ij}^{kl}(\mathbf{r})n_j|_s = 0 \quad (24)$$

$$p_{ij}^k(\mathbf{r})n_j|_s = 0 \quad (25)$$

In summary, the unit cell problems that must be solved for the 3D grid-reinforced smart composite structure with a single family of orthotropic reinforcements/actuators are given by Eqs. (20) and (21) in conjunction with Eqs. (22)-(25).

In order to solve the pertinent unit cell problems we perform a coordinate transformation of the global coordinate system $\{y_1, y_2, y_3\}$ into the new coordinate system $\{\eta_1, \eta_2, \eta_3\}$ shown in Fig. 3. With the new coordinate system we note that since the reinforcement is oriented along the η_1 coordinate axis, the problem at hand becomes independent of η_1 and depend only on η_2 and η_3 . As a result, the ensuing analysis becomes much easier.

Effective Elastic and Piezoelectric Coefficients

A scheme for the determination of the effective elastic and piezoelectric coefficients for 3D grid-reinforced composite structures with generally orthotropic reinforcements is given in detail in Kalamkarov et al. (2009b) and Hassan et al. (2009). It is noteworthy to mention that in the limiting particular case of 2D grid-reinforced structure with isotropic reinforcements the developed expressions for the effective elastic coefficients converge to those obtained earlier by Kalamkarov (1992).

With reference to Fig. 3, we begin by rewriting Eqs. (18), (22) and (24) in the $\{\eta_1, \eta_2, \eta_3\}$ coordinates to get:

$$b_{ij}^{kl} = C_{ijkl}(\mathbf{y}) + C_{ijmn} q_{pn} \frac{\partial N_m^{kl}(\mathbf{y})}{\partial \eta_p}, \quad (26)$$

$$\left(b_{ij}^{kl} q_{2j} n_2'(\mathbf{r}) + b_{ij}^{kl} q_{3j} n_3'(\mathbf{r}) \right) |_s = 0$$

Here, q_{ij} are the direction cosines characterizing the axes rotation (see Fig. 3); n_2' and n_3' are the components of the unit normal vector in the new coordinate system. Expanding Eq. (26) and keeping in mind the independency of the unit cell problem on η_1 yields:

$$b_{ij}^{kl} = C_{ijkl} + C_{ijm1}q_{21} \frac{\partial N_m^{kl}}{\partial \eta_2} + C_{ijm2}q_{22} \frac{\partial N_m^{kl}}{\partial \eta_2} + C_{ijm3}q_{23} \frac{\partial N_m^{kl}}{\partial \eta_2} + C_{ijm1}q_{31} \frac{\partial N_m^{kl}}{\partial \eta_3} + C_{ijm2}q_{32} \frac{\partial N_m^{kl}}{\partial \eta_3} + C_{ijm3}q_{33} \frac{\partial N_m^{kl}}{\partial \eta_3} \quad (27)$$

Apparently, Eqs. (26) and (27) can be solved by assuming a linear variation of the local functions N_m^{kl} with respect to η_2 and η_3 :

$$N_1^{kl} = \lambda_1^{kl} \eta_2 + \lambda_2^{kl} \eta_3, \quad N_2^{kl} = \lambda_3^{kl} \eta_2 + \lambda_4^{kl} \eta_3, \quad (28)$$

$$N_3^{kl} = \lambda_5^{kl} \eta_2 + \lambda_6^{kl} \eta_3,$$

where λ_i^{kl} are constants to be determined from the boundary conditions. Once these coefficients are determined, the coefficients b_{ij}^{kl} are found from the Eq. (27). In turn, these are used to calculate the effective elastic coefficients of the structure of Fig. 3 by integrating over the volume of the unit cell

$$\tilde{C}_{ijkl} = \frac{1}{|Y|} \int_Y b_{ij}^{kl} dv \quad (29)$$

Noting that b_{ij}^{kl} are constants, the effective elastic coefficients become

$$\tilde{C}_{ijkl} = \mu_f b_{ij}^{kl} \quad (30)$$

where μ_f is the volume fraction of the reinforcement within the unit cell. It can be proved in general case that the effective elastic coefficients \tilde{C}_{ijkl} maintain the same symmetry and convexity properties as their actual material counterparts C_{ijkl} , see Kalamkarov (1992).

The above derived effective moduli pertain to grid-reinforced structures with a single family of reinforcements. For structures with more than one family of reinforcements the effective moduli can be obtained by superposition. The effective elastic coefficients of a grid-reinforced structure with N families of generally orthotropic reinforcements will be given by:

$$\tilde{C}_{ijkl} = \sum_{n=1}^N V \mu_f^{(n)} b_{ij}^{(n)kl} \quad (31)$$

where the superscript (n) represents the n -th reinforcement family with the reinforcement volume fraction $\mu_f^{(n)}$.

Let us now proceed to calculation of the effective piezoelectric coefficients from the unit cell problem given by Eqs. (19), (23) and (25) which in coordinates $\{\eta_2, \eta_3, \eta_3\}$ becomes

$$p_{ij}^k = P_{ijk} - C_{ijmn} q_{pn} \frac{\partial M_m^k}{\partial \eta_p}, \quad (32)$$

$$\left(p_{ij}^k q_{2j} n_2'(r) + p_{ij}^k q_{3j} n_3'(r) \right) \Big|_s = 0$$

Keeping in mind independency on η_1 , Eq. (32) yields:

$$p_{ij}^k = P_{ijk} - (C_{ijm1}q_{21} \frac{\partial M_m^k}{\partial \eta_2} + C_{ijm2}q_{22} \frac{\partial M_m^k}{\partial \eta_2} + C_{ijm3}q_{23} \frac{\partial M_m^k}{\partial \eta_2} + C_{ijm1}q_{31} \frac{\partial M_m^k}{\partial \eta_3} + C_{ijm2}q_{32} \frac{\partial M_m^k}{\partial \eta_3} + C_{ijm3}q_{33} \frac{\partial M_m^k}{\partial \eta_3}) \quad (33)$$

It can be shown that Eq. (33) in conjunction with Eq. (32) can be solved by assuming a linearity of functions $N_m^k(\mathbf{y})$ in η_2 and η_3 :

$$M_1^k = \Sigma_1^k \eta_2 + \Sigma_2^k \eta_3, \quad M_2^k = \Sigma_3^k \eta_2 + \Sigma_4^k \eta_3, \quad (34)$$

$$M_3^k = \Sigma_5^k \eta_2 + \Sigma_6^k \eta_3,$$

where Σ_i^k are constants that can be determined from the boundary conditions. The functions given by Eqs. (33) and (34) are used to calculate the effective piezoelectric coefficients of the smart composite structure of Fig. 3 by integrating over the volume of the unit cell, which on account of Eqs. (17) and (19) yields

$$\tilde{P}_{ijk} = \frac{1}{|Y|} \int_Y p_{ij}^k dv \quad (35)$$

Since the local functions p_{ij}^k are constant, the effective piezoelectric coefficients become

$$\tilde{P}_{ijk} = \mu_f p_{ij}^k \quad (36)$$

where μ_f is the volume fraction of the actuators/reinforcement within the unit cell.

The effective piezoelectric coefficients derived above pertain to grid-reinforced smart composite structures with a single family of actuators/reinforcements. For structures with multiple families of inclusions the effective actuation coefficients can be obtained by superimposition. For instance, pertaining to a grid-reinforced smart composite structure with N families of actuators/reinforcements the effective coefficients will be given by

$$\tilde{P}_{ijk} = \sum_{n=1}^N \mu_f^{(n)} p_{ij}^{(n)k}, \quad (37)$$

where the superscript (n) represents the n th reinforcement/actuator family, as in the above Eq. (31).

Examples of Smart Grid-Reinforced Composite Structures

The developed micromechanical model will now be used to analyze three different practically important examples of smart 3D grid-reinforced composite structures with orthotropic actuators/reinforcements, see Hassan et al. (2009, 2011). The first example, structure S_1 is shown in Fig. 2. It has three families of orthotropic actuators/reinforcements, each family oriented along one of the coordinate axes. The second example, structure S_2 is shown in Fig. 4. It is formed by a conical array of orthotropic reinforcements/actuators.

The third example structure S_3 is shown in Fig. 5. It has a unit cell formed by three actuators/reinforcements, two of them extended diagonally across the unit cell between two diametrically opposite vertices while the third reinforcement is spun between the middle of the bottom edge and the middle of the top edge on the opposite face. The effective elastic and piezoelectric coefficients for the above introduced three structures are calculated on the basis of Eqs. (31) and (37). Although the obtained analytical results are too lengthy to be reproduced here, the plots of some of these effective coefficients vs. reinforcement volume fraction or vs. the inclination of the reinforcements with the y_3 axis are shown below, see Kalamkarov et al. (2009b) and Hassan et al. (2009, 2011) for the details.

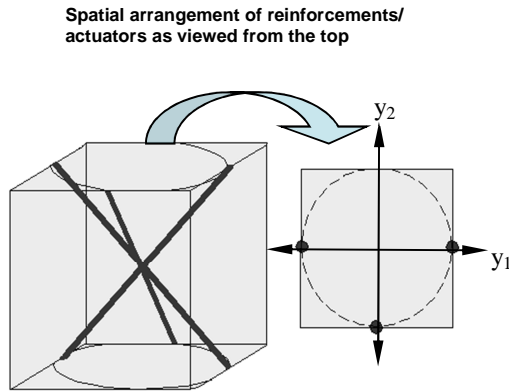


Figure 4. Unit cell of smart composite structure S_2 with conical arrangement of orthotropic reinforcements/actuators.

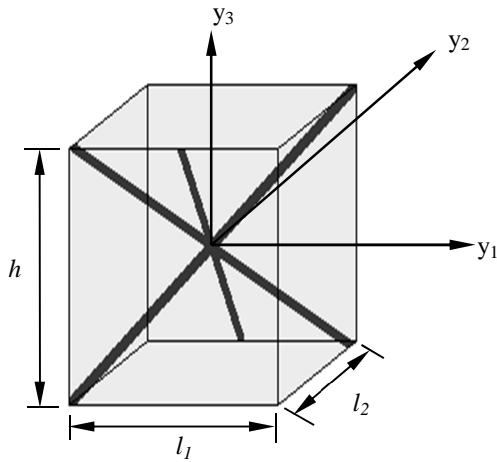


Figure 5. Unit cell of smart composite structure S_3 with diagonally arranged orthotropic actuators/reinforcements.

We assume that the actuators/reinforcements are made of piezoelectric material PZT-5A with the following material properties (see Cote et al., 2002):

$$\begin{aligned} C_{11}^{(p)} &= C_{22}^{(p)} = 121.0 \text{ GPa}, & C_{33}^{(p)} &= 111.0 \text{ GPa}, \\ C_{12}^{(p)} &= 75.4 \text{ GPa}, & C_{13}^{(p)} &= C_{23}^{(p)} = 75.2 \text{ GPa}, \\ C_{44}^{(p)} &= 22.6 \text{ GPa}, & C_{55}^{(p)} &= C_{66}^{(p)} = 21.1 \text{ GPa}, \\ P_{13}^{(p)} &= P_{23}^{(p)} = -5.45 \times 10^{-6} \text{ C/mm}^2, \\ P_{33}^{(p)} &= 1.56 \times 10^{-5} \text{ C/mm}^2, & P_{42}^{(p)} &= P_{51}^{(p)} = 2.46 \times 10^{-5} \text{ C/mm}^2. \end{aligned}$$

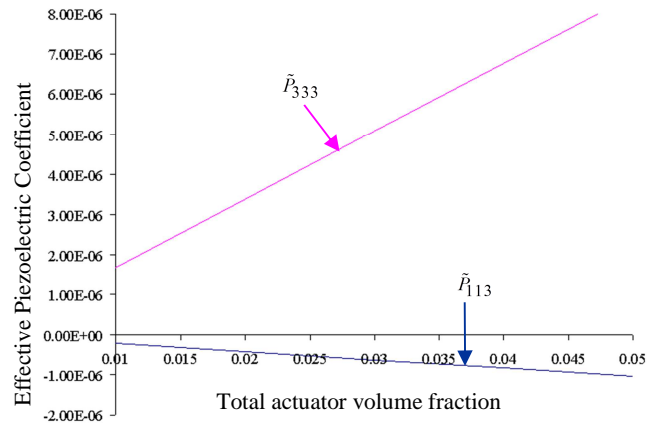


Figure 6. Plot of \tilde{P}_{113} and \tilde{P}_{333} effective piezoelectric coefficients vs. actuator volume fraction for structure S_1 .

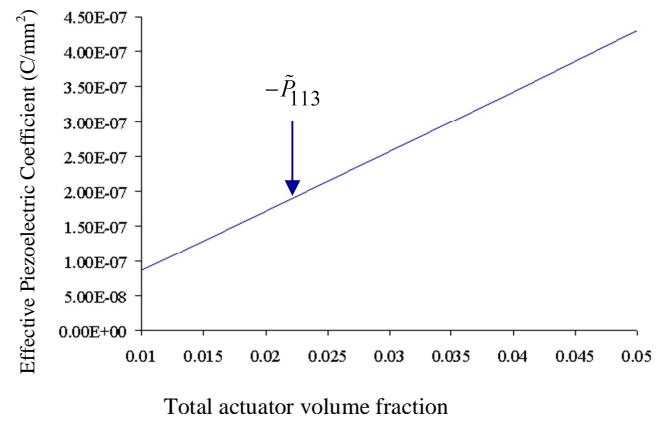


Figure 7. Plot of $-\tilde{P}_{113}$ effective piezoelectric coefficient vs. actuator volume fraction for structure S_2 (actuators oriented at 33.7° to the y_3 axis).

We start by providing numerical results for the effective coefficients of structure S_1 shown in Fig. 2. Typical piezoelectric coefficients are plotted vs. volume fraction in Fig. 6. As expected, these coefficients increase in magnitude as the volume fraction increases. One also observes from Fig. 6 that the values of \tilde{P}_{333} are larger than \tilde{P}_{113} for a given volume fraction, which is to be expected because the former refers to the stress response in the direction y_3 in which electric field is applied.

We now turn our attention to structure S_2 of Fig. 4. Typical effective piezoelectric coefficients are plotted vs. the total volume fraction of the actuators/reinforcements within the unit cell in Figs. 7 and 8. As expected, the plots show an increase in the effective piezoelectric coefficients as the overall volume fraction increases. And it is seen from Figs. 6 and 7 that the magnitude of the coefficient \tilde{P}_{113} (which refers to the stress response of the structure in the y_1 -direction when an external field is applied in the y_3 -direction) is larger for Structure S_1 than for Structure S_2 . This is expected and is attributed to the geometry of the unit cells. Figure 6 refers to structure S_1 with some actuators/reinforcements oriented entirely in the y_3 direction. Figure 7 refers to structure S_2 where none of the reinforcements are oriented in the y_3 -direction (all 3 actuators/reinforcements are oriented at about 34° to the y_3 axis). Consequently, the stress response of structure S_2 in the y_1 direction

when a voltage is applied in the y_3 direction is smaller and so is the corresponding effective coefficient \tilde{P}_{113} .

It is also of interest to analyze the variation of the effective coefficients of structure S_2 vs. the angle of inclination of the actuators/reinforcements to the y_3 axis. As this angle increases, the actuators/reinforcements are oriented progressively closer to y_1 - and y_2 -axes, and, consequently, further away from the y_3 axis. Thus, one expects a corresponding increase in the values of effective coefficients, as it is seen in the Fig. 8 plotting \tilde{P}_{113} and \tilde{P}_{223} .

We now turn our attention to structure S_3 shown in Fig. 5 and we will present graphically some of the effective piezoelectric coefficients vs. the relative height of the unit cell, see Fig. 9. The relative height is defined as the ratio of the height to the length of the unit cell. The width of the unit cell and the cross-sectional area of the reinforcements/actuators stay the same. It is noted that when the relative height of the unit cell is increased the total volume fraction of the reinforcements/actuators as well as the orientation angle between these actuators and y_3 -axis will decrease. This has

very interesting consequences on the effective coefficients. In particular, decrease of the angle of inclination of the actuators with the y_3 axis will reduce the stiffness in y_1 and y_2 directions because the actuators are oriented further away from the y_1 - y_2 plane. The simultaneous decrease in the overall actuator volume fraction makes this effect even more pronounced. These trends are clearly visible in Fig. 9 for the coefficients \tilde{P}_{112} and \tilde{P}_{222} . However, as far as the stiffness in the y_3 -direction is concerned the two factors that accompany the increase in the relative height of the unit cell are in direct competition with one another. That is, decreasing the angle of inclination of the actuators with y_3 -axis increases such coefficients as \tilde{P}_{332} and \tilde{P}_{333} , but decreasing the overall actuator volume fraction naturally reduces the magnitude of these coefficients. As Fig. 9 shows, the former effect dominates the latter one, especially for low to moderate values of the relative height of the unit cell. However, after a certain point, the two factors tend to compensate each other, so that the value of \tilde{P}_{332} increases at a modest rate.

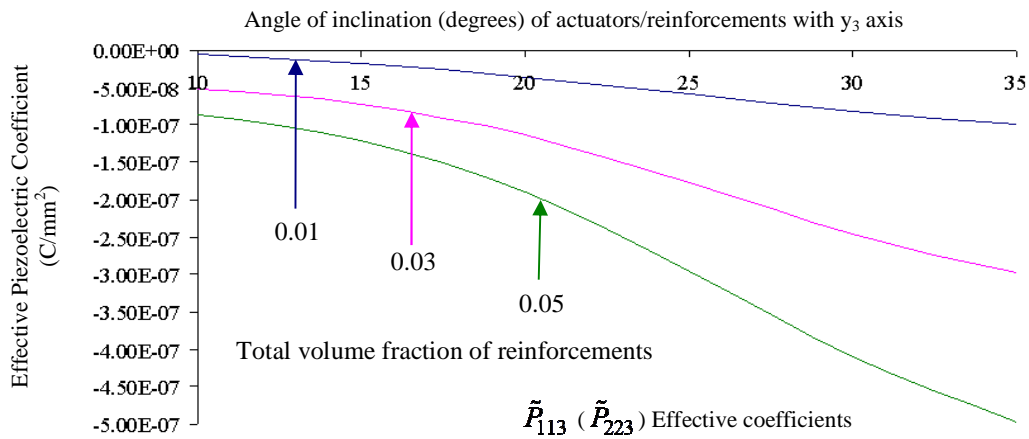


Figure 8. Plot of \tilde{P}_{113} ($= \tilde{P}_{223}$) effective piezoelectric coefficient vs. inclination of actuators/reinforcements with the y_3 axis for different volume fractions (structure S_2).

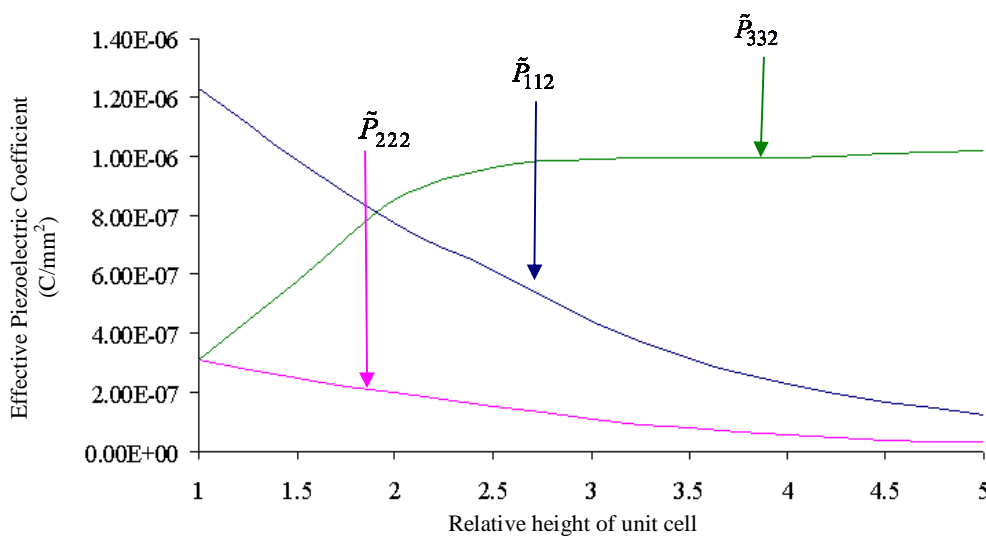


Figure 9. Plot of \tilde{P}_{112} , \tilde{P}_{222} , and \tilde{P}_{332} effective piezoelectric coefficients vs. relative height of unit cell for structure S_3 .

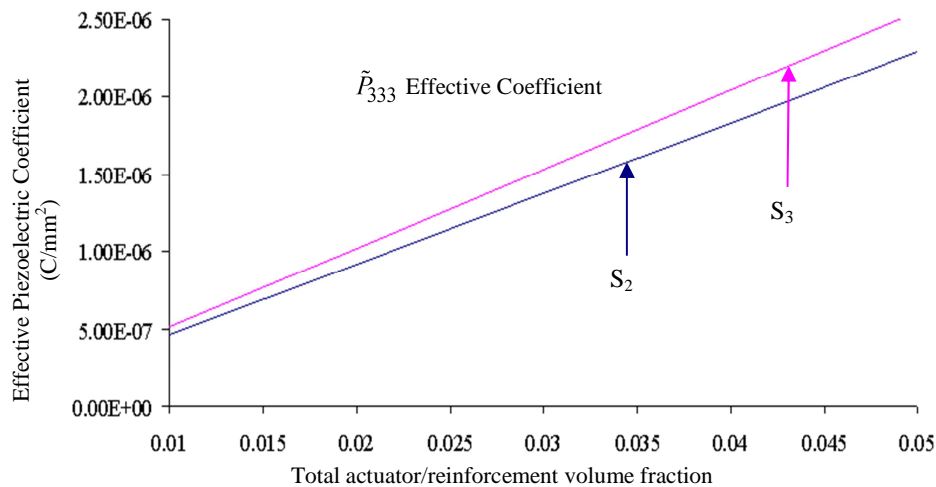


Figure 10. Plot of \tilde{P}_{333} effective piezoelectric coefficient vs. total volume fraction for structures S_2 and S_3 .

Finally, we compare the typical effective coefficients of structures S_2 and S_3 by varying the total volume fraction of the actuators/reinforcements but keeping the same dimensions of the respective unit cells, see Fig. 10. Under these circumstances structure S_3 has higher effective piezoelectric coefficient \tilde{P}_{333} than structure S_2 . This is attributed to the different angles of inclination of the actuators/reinforcements to the y_3 axis.

The above discussed examples demonstrate that the derived micromechanical model allows developing a smart composite structure with the desirable combination of effective properties via selection of relevant material and geometric parameters such as number, type and cross-sectional dimensions of the actuators/reinforcements, relative dimensions of the unit cell, and the spatial orientation of the actuators/reinforcements.

We also note that the advantage of our model is that the effective coefficients can be computed easily without the need of time consuming numerical (such as finite element) calculations, see Hassan et al. (2011) where the analytical and finite element models are compared.

Conclusions

Smart composite structures reinforced with a periodic grid of generally orthotropic cylindrical reinforcements that also exhibit piezoelectric behavior are considered. The review of micromechanical modeling of these smart structures based on the application of the asymptotic homogenization method is presented. The micromechanical model decouples the original boundary-value problem into a simpler set of problems called the unit cell problems which describe the elastic and piezoelectric effective properties of the smart 3D grid-reinforced composite structures. By means of the solution of the unit cell problems the explicit expressions for the effective elastic and piezoelectric coefficients are obtained. The general orthotropy of the reinforcement material is important from the practical viewpoint, and makes the mathematical analysis much more complicated. It is worth mentioning that even though the analysis presented is applied to the piezoelectric material, the model derived accommodates equally well any smart composite structure exhibiting some general transduction characteristic that can be used to induce strains or stresses in some controlled manner. The developed micromechanical model is applied to different examples of orthotropic smart composite structures with cubic, conical and

diagonal actuators/reinforcements arrangements. It is shown in these examples that the micromechanical model provides a complete flexibility in designing a 3D smart grid-reinforced composite structure with desirable piezoelectric characteristics to conform to a particular engineering application by tailoring certain material and/or geometric parameters. Examples of such parameters include the type, number, material and cross-sectional characteristics and relative orientations of the actuators and reinforcements.

Acknowledgements

The authors acknowledge the support of the Natural Sciences and Engineering Research Council of Canada (NSERC), the Brazilian Research Agencies CNPq, CAPES, FAPERJ and the National Institute of Science and Technology on Smart Structures for Engineering (INCT-EIE). The support of the Air Force Office of Scientific Research (AFOSR) is also acknowledged.

References

- Andrianov, I.V., Danishevs'kyy, V.V. and Kalamkarov, A.L., 2006, "Asymptotic justification of the three-phase composite model", *Compos. Struct.*, Vol. 77, pp. 395-404.
- Bakhvalov, N.S. and Panasenko, G.P., 1989, "Averaging Processes in Periodic Media. Mathematical Problems in Mechanics of Composite Materials", Kluwer, Dordrecht.
- Bensoussan, A., Lions, J.L. and Papanicolaou, G., 1978, "Asymptotic Analysis for Periodic Structures", North-Holland, Amsterdam.
- Budiansky, B., 1965, "On the elastic moduli of some heterogeneous materials", *J. Mech. Phys. Solids*, Vol. 13, pp. 223-227.
- Challagulla, K.S., Georgiades, A.V. and Kalamkarov, A.L., 2007, "Asymptotic homogenization modeling of thin network structures", *Compos. Struct.*, Vol. 3, pp. 432-444.
- Challagulla, K.S., Georgiades, A.V., Saha, G.C. and Kalamkarov, A.L., 2008, "Micromechanical analysis of grid-reinforced thin composite generally orthotropic shells", *Composites, Part B: Eng.*, Vol. 39, pp. 627-644.
- Christensen, R.M., 1990, "A critical evaluation for a class of micromechanics models", *J. Mech. Phys. Solids*, Vol. 38, pp. 379-404.
- Cote, F., Masson, P. and Mrad, N., 2002, "Dynamic and static assessment of piezoelectric embedded composites", *Proceedings of the SPIE*, Vol. 4701, pp. 316-325.
- Drugan, W.J. and Willis, J.R., 1996, "A micromechanics-based nonlocal constitutive equation and estimates of representative volume element size for elastic composites", *J. Mech. Phys. Solids*, Vol. 44, pp. 497-524.

- Hashin, Z. and Rosen, B.W., 1964, "The elastic moduli of fiber-reinforced materials", *J. Appl. Mech.*, Vol. 31, pp. 223-232.
- Hassan, E.M., 2011, "Modeling of 3D grid-reinforced smart anisotropic composite structures", Lambert Acad. Publ., ISBN 978-3-8433-6651-9.
- Hassan, E.M., Georgiades, A.V., Savi, M.A. and Kalamkarov, A.L., 2011, "Analytical and numerical analysis of 3D grid-reinforced orthotropic composite structures", *Int. J. Eng. Sc.*, Vol. 49, pp. 589-605.
- Hassan, E.M., Kalamkarov, A.L., Georgiades, A.V. and Challagulla, K.S., 2009, "An asymptotic homogenization model for smart 3D grid-reinforced composite structures with generally orthotropic constituents", *Smart Materials and Structures*, Vol. 18, No. 7, 075006 (16pp).
- Georgiades, A.V., Challagulla, K.S. and Kalamkarov, A.L., 2006, "Modeling of the thermopiezoelectric behavior of prismatic smart composite structures made of orthotropic materials", *Composites, Part B: Eng.*, Vol. 37, pp. 569-582.
- Kalamkarov, A.L., 1992, "Composite and Reinforced Elements of Construction", Wiley, Chichester, N.Y.
- Kalamkarov, A.L. and Georgiades, A.V., 2002a, "Modeling of smart composites on account of actuation, thermal conductivity and hygroscopic absorption", *Composites, Part B: Eng.*, Vol. 33, pp. 141-152.
- Kalamkarov, A.L. and Georgiades, A.V., 2002b, "Micromechanical modeling of smart composite structures", *Smart Materials Struct.*, Vol. 11, pp. 423-434.
- Kalamkarov, A.L., Andrianov, I.V. and Danishevs'kyi, V.V., 2009a, "Asymptotic homogenization of composite materials and structures", Transactions of the ASME, *Applied Mechanics Reviews*, Vol. 62, No. 3, pp. 030802-1-030802-20.
- Kalamkarov, A.L., Georgiades, A.V., Challagulla, K.S. and Saha, G.C., 2006, "Micromechanics of smart composite plates with periodically embedded actuators and rapidly varying thickness", *J. Thermoplastic Composite Mater.*, Vol. 19, pp. 251-276.
- Kalamkarov, A.L., Hassan, E.M., Georgiades, A.V., 2010, "Micromechanical modeling of 3D grid-reinforced composite structures and nanocomposites", *Journal of Nanostructured Polymers and Nanocomposites*, Vol. 6, Issue 1, pp. 12-20.
- Kalamkarov, A.L., Hassan, E.M., Georgiades, A.V. and Savi, M.A., 2009b, "Asymptotic homogenization model for 3D grid-reinforced composite structures with generally orthotropic reinforcements", *Compos. Struct.*, Vol. 89, pp. 186-196.
- Kalamkarov, A.L. and Kolpakov, A.G., 1997, "Analysis, Design and Optimization of Composite Structures", Wiley, Chichester, N.Y.
- Kalamkarov, A.L. and Kolpakov, A.G., 2001, "A new asymptotic model for a composite piezoelectric plate", *Int. J. Solids Struct.*, Vol. 38, pp. 6027-6044.
- Kalamkarov, A.L. and Liu, H.Q., 1998, "A new model for the multiphase fiber-matrix composite materials", *Composites, Part B: Eng.*, Vol. 29, pp. 643-653.
- Mori, T. and Tanaka, K., 1973, "Average stress in matrix and average energy of materials with misfitting inclusions", *Acta Metallurgica et Materialia*, Vol. 21, pp. 571-574.
- Saha, G.C., Kalamkarov, A.L. and Georgiades, A.V., 2007a, "Effective elastic characteristics of honeycomb sandwich composite shells made of generally orthotropic materials", *Composites, Part A: Appl. Sci. and Manuf.*, Vol. 38, pp. 1533-1546.
- Saha, G.C., Kalamkarov, A.L. and Georgiades, A.V., 2007b, "Micromechanical analysis of effective piezoelectric properties of smart composite sandwich shells made of generally orthotropic materials", *Smart Mater. Struct.*, Vol. 16, pp. 866-883.
- Sanchez-Palencia, E., 1980, "Non-Homogeneous Media and Vibration Theory", Lecture Notes in Physics, Springer, Berlin.
- Sendekyj, G.P., 1974, "Mechanics of Composite Materials", Academic Press, New York.
- Vinson, J.R. and Sierokowski, R.L., 1986, "The Behavior of Structures Composed of Composite Materials", Kluwer, Dordrecht.